Infrared Physics and Technology 98 (2019) 223–229

Contents lists available at ScienceDirect

Infrared Physics & Technology

journal homepage: www.elsevier.com/locate/infrared

Regular article

Evaluation of an ancient cast-iron Buddha head by step-heating infrared thermography

Xiaoli Li[a], Ning Tao[b,*], J.G. Sun[b,c], Yong Lei[d], Liang Qu[d], Fei Gao[d], Yi He[e], Guan Wang[e], Lichun Feng[b]

[a] School of Logistics, Beijing Wuzi University, Beijing 101149, China
[b] Beijing Key Lab for Terahertz Spectroscopy and Imaging, Key Lab of Terahertz Optoelectronics, Ministry of Education, and Beijing Advanced Innovation Center for Imaging Technology, Department of Physics, Capital Normal University, Beijing 100048, China
[c] Argonne National Laboratory, Argonne, IL 60439, USA
[d] The Palace Museum, Beijing 100009, China
[e] Beijing Waiteksin Advanced Technology Co. Ltd, Beijing 100048, China

ARTICLE INFO

Keywords:
Step-heating
Infrared thermography
Cultural relics
Wall thickness

ABSTRACT

The authors report on the development of a step-heating infrared thermography method for nondestructive evaluation of a cast-iron Buddha head made in the Song Dynasty (AD 960–1279) in China. In particular, this method measures the wall-thickness distribution, which can be used as an indicator for the condition of the object. Unlike other areas of analysis, inspection of cultural relics requires special attention to safety. To avoid the heat shock associated with traditional flash thermography, a step-heating method with a mild heating process is considered to be more acceptable for evaluating cultural relics made from various materials. Before application to inspection of the Buddha head, a numerical analysis and experimental tests were performed to verify the accuracy of this step-heating thickness measurement method. Finally, thickness images of the Buddha head were acquired and analyzed. The step-heating thickness measurement method has a high accuracy and can be safely used for inspecting cultural relics.

1. Introduction

China has a long and unique history preserved in countless cultural relics. Therefore, protecting this inheritance is important. Most relics need to be non-destructively inspected and evaluated before a reasonable preservation plan can be developed. Many nondestructive evaluation techniques have been applied in this area. For example, X-ray diffraction (XRD) has been used to analyze the mechanism of corrosion of metallic relics, examine weathering products of stone, and sometimes to analyze materials of paintings [1]; Radar, ultrasonic and impact-echo analyses have been applied to inspect concrete and masonry structures [2]; and Raman spectroscopy is capable of detecting stratification of artworks [3]. In some circumstances, minimal destructive analysis of relics is allowed to obtain important information required to better protect the object; however, in most instances, the testing methods must be nondestructive and preserve the sample. Thus, many common contact techniques are not appropriate for evaluating relics.

Thermal imaging is a non-contact and nondestructive method, which can determine the subsurface structures or defects of objects by analyzing their surface temperature variation and distribution. This technique has been successfully applied to many areas, such as aerospace, petroleum and petrochemical, electric power, and construction [4–8]. In recent years, thermal imaging has been applied to studying cultural relics [9], focused mainly on ancient architecture [10], rocks [11,12], paintings [1,13–16], wooden and metal objects [17–20]. For a test object in thermal equilibrium with its surroundings, a kind of controlled excitation is needed to generate thermal signatures related to the internal material. This process is usually termed active infrared thermography. Many excitation methods have been developed including flash lamps, lasers, halogen lamps, LED lamps, eddy currents, and ultrasonic pulses [14–23]; among these flash lamps are most commonly used for both qualitative [15] and quantitative [24–27] inspections. However, a flash lamp supplies a large amount of energy in a short time period, e.g., 1–5 ms [28]. This impulse may cause a temperature increase of tens to more than a hundred of degrees at the heated surface, which can be harmful to precious objects. In addition, a flash lamp requires a large and heavy power supply, which makes it inconvenient for field applications. By comparison, step-heating methods, e.g., based on a halogen lamp, provide a mild heating process that is more appropriate for evaluating cultural relics in field

* Corresponding author.

https://doi.org/10.1016/j.infrared.2019.03.017
Received 30 November 2018; Received in revised form 18 March 2019; Accepted 18 March 2019
Available online 19 March 2019
1350-4495/

conditions. Besides the step-heating, there are other excitation methods which provide low heating intensity, such as lock-in and others, although they require substantially more instrumentation [14,17,22].

With regard to metal artifacts, corrosion monitoring [20], manufacturing processes [19], ancient materials [18], and condition evaluation [18–20] have become hot topics of research. These aspects are often interrelated with each other. This study aims to develop a step-heating infrared thermography method for measuring the wall-thickness distribution of a cast-iron Buddha head made in the Song dynasty (About 1000 years ago). Cast-iron technology was developed more than a thousand years earlier than that in Europe [29]. Among artifacts produced in the 1400 years from the beginning of the Northern and Southern Dynasties (AD 420-589) to the middle of the Qing Dynasty (CE 1616-1912), a total of 619 pieces of ancient large-scale cast iron have been studied to date, of which 22 are extra-large weighing more than 10 tons [30]. These include Buddha statues, portraits, lions, cows, clocks, towers, stoves, and cannons. Most of the artifacts are iron castings with irreplaceable artistic value. The quality of the art work and casting technology level are very high. China's large cast-iron cultural relics are also the first of their kind in the world [29,30]. As a physical parameter that indicate the condition of these relics, the wall-thickness distribution and its measurement are meaningful for both cultural relic preservation researchers and for investigating ancient casting processes. For preservation purposes, if the wall thickness of the Buddha head is known, it is possible to avoid concentration of force in thinner areas during transportation and to develop targeted preservation plans. Additionally, investigations of ancient casting processes can provide more information on these ancient artworks. However, safety is always the most important thing for cultural relics inspection. Although the advantage of the low heating intensity in the step-heating method is less important for evaluating cast-iron objects, the developed method may also be applied to evaluate other cultural relics made from other materials that are more sensitive to temperature changes.

This paper is organized as follows. In the next section, the step-heating thickness method is introduced. Its precision was verified by analytical simulations and experimental testing. Then, the method was applied to measure the wall-thickness distributions of a cast-iron Buddha head and the effectiveness of the method was discuss.

2. Methods

2.1. Principle of step-heating thermography

The transmission step-heating setup applied in this study is shown in Fig. 1. In the basic test configuration, the sample is a semi-infinite flat plate with a thickness L and the infrared camera and the heating source are placed at either side of the sample. The heating source supplies a

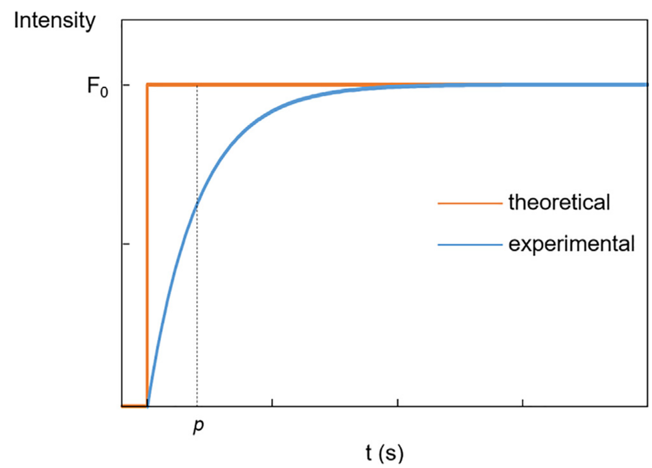

Fig. 2. Ideal intensity variation of a step-heating source.

step-heating excitation to the back surface at $z = L$, while the infrared camera captures the temperature transient of the front surface at $z = 0$ before and after the heating. The start heating time is set to be zero. When heating starts, the temperature of the heated surface increases instantly; the energy then conducts to the inner areas; and finally reaches the other side of the sample to be detected by the infrared camera. Because most of the heat conduction occurs in the depth direction, a 1D formulation can be used to model this heat transfer process.

The governing equation for heat conduction within the sample is:

$$\rho c\frac{\partial T(z,t)}{\partial t} = k\frac{\partial^2 T(z,t)}{\partial z^2}, \tag{1}$$

where z is the depth direction of the sample, as shown in Fig. 1, ρ, c, k are respectively the density, specific heat, and thermal conductivity of the material, and $T(z, t)$ is the temperature at depth z and time t. The authors further assume that the initial temperature of the sample is zero $T(z, 0) = 0$, $(0 \leqslant z \leqslant L)$ and all the boundaries are insulated.

For perfect step-heating with a heat flux F_0, as shown in Fig. 2, its formulation is:

$$F(\mathrm{t}) = \begin{cases} F_0, & (t \geqslant 0) \\ 0, & (t < 0) \end{cases}, \tag{2}$$

The function of the temperature variation with time and depth can be derived from the governing Eq. (1) and the initial and boundary conditions [31]. After a step-heating source was applied to the back surface of the sample, the temperature of the front surface can be expressed as [32],

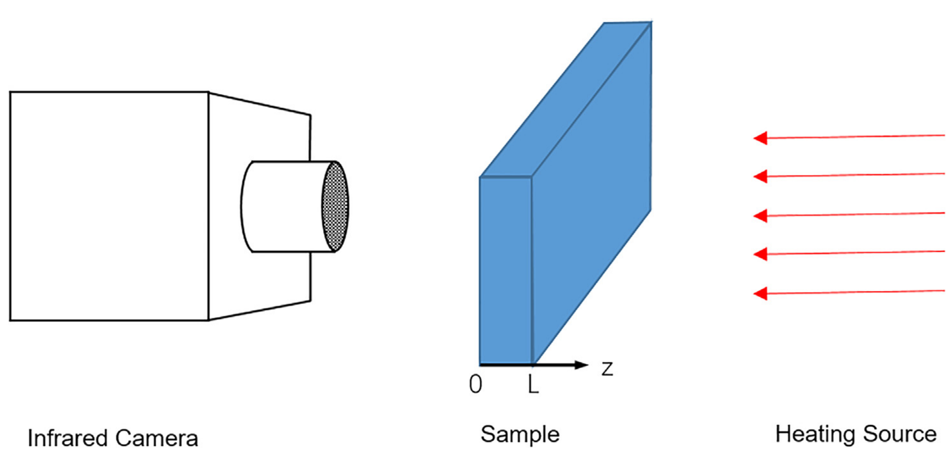

Fig. 1. Schematic diagram of the experimental system.

Table 1
Parameters of the stainless steel used in the ANSYS analysis.

	Conductivity W/(m·K)	Specific heat J/(kg·K)	Density kg/m^3
Stainless steel	14.2	489	7930

$$T(0,\,t)=\frac{F_0L}{k}\left[\frac{\alpha}{L^2}t-\frac{1}{6}-\frac{2}{\pi^2}\sum_{n=1}^{\infty}\frac{(-1)^n}{n^2}\exp\left(-\frac{n^2\pi^2\alpha t}{L^2}\right)\right]. \tag{3}$$

Setting $\frac{F_0L}{k}=f_1$ and $\frac{\alpha}{L^2}=f_2$, Eq. (3) can be rewritten as:

$$T(0,\,t)=f_1\left[f_2\,t-\frac{1}{6}-\frac{2}{\pi^2}\sum_{n=1}^{\infty}\frac{(-1)^n}{n^2}\exp(-f_2 n^2\pi^2 t)\right]. \tag{4}$$

This function has four parameters$F(T,\,t,\,f_1,\,f_2)$. The temperature T and time t can be obtained from an experiment or a numerical simulation, and f_1, f_2 can be calculated by a nonlinear fitting method, as described in [33]. Once f_2 is determined, the thickness L becomes known with a given thermal diffusivity α, or vice versa.

2.2. Analytical validation

To validate the accuracy of the step-heating thickness measurement method under ideal circumstances, a finite element analysis was performed using the ANSYS software. For consistency with the real test sample, a stainless-steel material was applied here. The material parameters used in the simulation are shown in Table 1. Six models with different thicknesses varying from 5 to 50 mm (see Table 2) were built and calculated. As shown in Fig. 3, the modeled geometry was a square plate with a lateral width 5 times as great as the thickness for each model. Therefore, the grid length became larger as the thickness increased, and surface refinements were applied to all the models. The heat flux was 2500 W/m^2 in all simulations.

The duration of the simulations was dependent upon the plate thickness. According to our previous experimental work, if the data acquisition length (or duration) is longer than the half-rise time $t_{1/2}$, which is $0.14L^2/\alpha$, the fitting results will not be notably affected [33] (here the thermal diffusivity α can be obtained with the parameters in Table 1: $\alpha = k/\rho c = 3.66\,\mathrm{mm}^2/\mathrm{s}$). Therefore, the calculation lengths for all models (except for M6, which was equal to $t_{1/2}$) were set to be 2 times as long as $t_{1/2}$, based on their own thickness.

The temperature-time data of the unheated surface calculated from the six models were fitted with Eq. (4) based on the nonlinear fitting algorithm described in our previous work [32,33]. As shown in Fig. 4, excellent fittings were obtained for the calculated data of all models. From the fitted parameter $f_2 = \alpha/L^2$ and the known thermal diffusivity $\alpha = 3.66\,\mathrm{mm}^2/\mathrm{s}$, the thicknesses of all models were calculated and are listed in Table 2.

As Table 2 shows, all the fitted thicknesses had high accuracy with errors no greater than -0.3%. Furthermore, the error of the result was stable, and not influenced by the thickness of the object. Thus, the method should be reliable for testing thick objects.

2.3. Experimental validation

In the experimental setup, a cooled infrared camera SC4000 whose parameters is listed in the Table 3 was used. A 500-W halogen lamp was used as the heat source. A stainless-steel (SS304) step-wedge sample was used in this experimental validation. As illustrated in Fig. 5, the sample had four different thicknesses: i.e., 5.09, 11.38, 17.76, and 24.08 mm. Because the surface of the sample had a low infrared emissivity and high optical reflection, a very thin graphite coating (< 1 µm) was applied to both sides of the sample surface to improve emissivity. According to the literature, the thermal diffusivity of SS304 is

Table 2
Fitting results of analytical data.

Real thickness (mm)	5	10	15	20	30	50
Fitted thickness (mm)	4.99	9.99	14.99	19.96	29.94	49.86
Error (%)	−0.20	−0.10	−0.07	−0.20	−0.20	−0.28

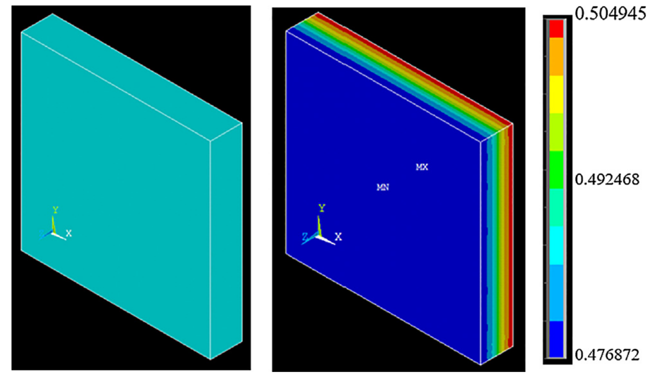

Fig. 3. Example of model and resulting images from ANSYS analysis.

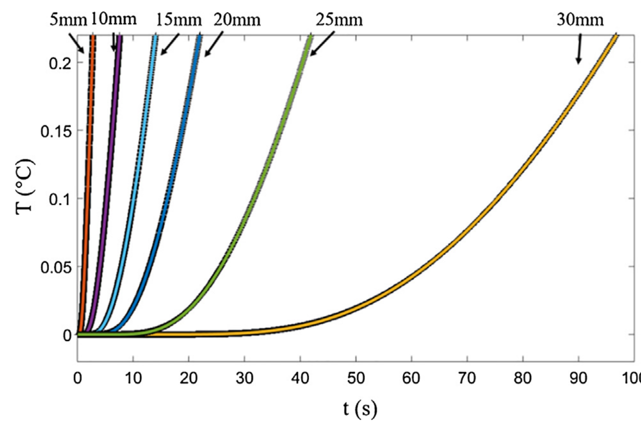

Fig. 4. ANSYS results and their fitting curves of models.

Table 3
Parameters of the infrared cameras used in this study.

Camera	SC4000	VarioCAM hr
Detector	Cooled	Uncooled
Focal plane array size	320 × 256	640 × 480
Spectral range	3–5 µm	7.5–14 µm
NETD	25 mK nominal or 18 mK at typical situation	30 mK (@30 °C)

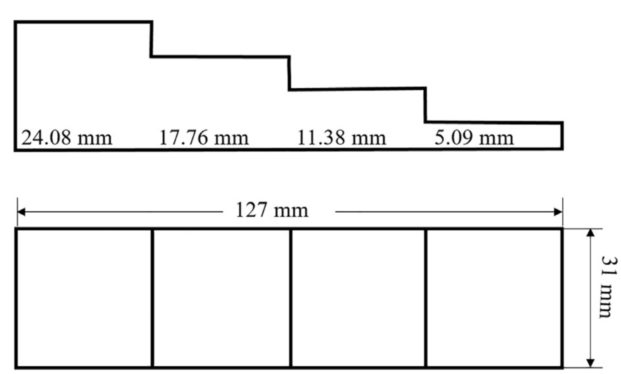

Fig. 5. Schematic diagram of the sample.

3.66 mm^2/s at room temperature [34,35]. In the experiment, the frame capture rate and the total test duration were balanced for the different sample thicknesses. This is because the speed of the temperature rise on the imaged surface is inversely related to the sample thickness. Thus, narrow steps require a high capture rate and short capture time, whereas thick steps require a long capture time and low capture rate. To balance these factors, the infrared camera frequency and the capture duration were set to 200 Hz and 25 s for each experiment; a total of three experiments were performed.

Compared with the ideal step-heating source, Eq. (2), the halogen lamp used in the experiment required a long time (tens to hundreds of milliseconds) to reach to a constant light intensity as shown in Fig. 2. This intensity rise time of the real heat source affected the surface temperature, which in turn affected the thickness measurements. Therefore, the surface temperature expression in Eq. (4) for an ideal step-heating source should be corrected according to the real heating curve:

$$F(t) = F_0(1 - e^{-t/p}), \tag{5}$$

where p is the temperature rising time of the heating source. Our previous work has also derived this corrected surface temperature expression as [31]:

$$T(0,t) = f_1\{f_2 t - \frac{1}{6} - pf_2(1 - e^{-t/p}) - 2\sum_{n=1}^{\infty} \frac{(-1)^n}{1 - n^2\pi^2 pf_2}\left[\frac{e^{-n^2\pi^2 f_2 t}}{n^2\pi^2} - pf_2 e^{-t/p}\right]\} \tag{6}$$

The experimental data were fitted with Eq. (6) and the fitting curves for four representative points are illustrated in Fig. 6. At the two thinner steps, the energy penetrated at short times and the temperature increased rapidly. At the two thicker steps the temperature changed more slowly and failed to reach the linear domain at the end of the 25-s data acquisition time. The experimental data length in the fitting process was 2 times as long as $t_{1/2}$ for the three thinner steps but only 1 times as long as $t_{1/2}$ for the thickest step ($t_{1/2} = 22.2$ s). After fitting each pixel of the data, the thickness image was obtained, as shown in Fig. 7. The center area, illustrated as a white square in Fig. 7, was selected to calculate the average predicted thickness for every step and the results are listed in Table 4. The predicted thickness for the thinnest step had the largest error of 5.09%; the error decreased sharply for the second thinnest step to 1.4%; and the error decreased to −0.1% for the thickest step. Thus, the results were reasonable for all the steps and particularly thicker ones. Notably, the error behavior is unlike that of flash thermography, where measurement accuracy degrades with sample thickness. The increase of the measurement error for thinner steps was due to the assumption of a constant heating time p. However, detailed measurements show that the real heating curve near t = 0 is not modeled well by a constant p in Eq. (5). Additional studies on this aspect are underway and the results will be published elsewhere.

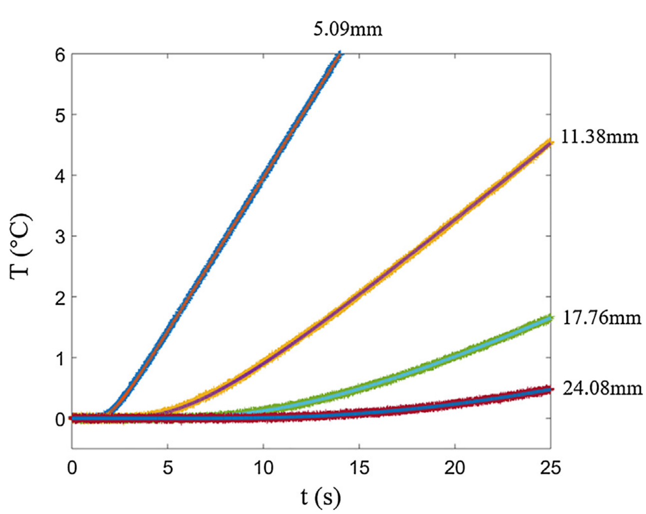

Fig. 6. Experimental data for the step-wedge sample.

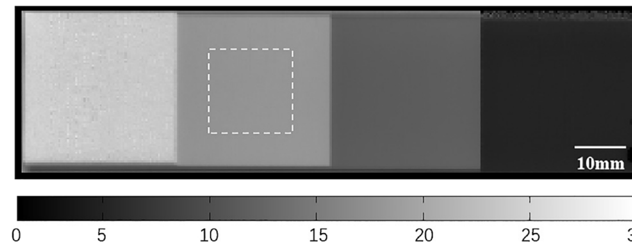

Fig. 7. Measured thickness image of the step-wedge sample (unit of thickness scale in mm).

Table 4
Predicted thickness and error analysis for the step-wedge sample.

L (mm), real	24.08	17.76	11.38	5.09
Predicted	24.06 ± 0.25	17.96 ± 0.06	11.54 ± 0.08	5.38 ± 0.04
Error (%)	−0.1	1.1	1.4	5.6

3. Buddha head application

Fig. 8a shows a picture of the cast-iron Buddha head made in the Song Dynasty, which now belongs to the Palace Museum in Beijing, China. The high quality of the sculpted art and casting technique give this particular artifact a high historical heritage value. This Buddha head is approximately 35 cm long and the diameter of its cross section is approximately 20 cm. The maximum thickness is approximately 3 cm [36]. Overall the sculpture is in good condition; however, some surface areas have minor rusting. The head has a hollow structure and the wall thickness ranges from several to tens of millimeters according to the features of the head.

In this experiment taken in the Palace Museum, a 14 cm long 800 W halogen light tube was used as the heat source, since the light intensity will affect only the fitting parameter f_1 in Eq. (6) which has no influence to the accuracy of the thickness measurement derived from the fitting parameter f_2. The Buddha head was excited from the inside surface [37]. A portable uncooled camera VarioCAM hr was used to capture the temperature variation of the outside surface. Its parameters are listed in Table 3. The capture rate in this experiment was 50 Hz and the test duration was ~6 s. Fig. 8b shows a typical raw thermal image from the experiment. Such images can be used for qualitative assessment of the wall-thickness variation because thinner sections of wall will transfer heat more quickly giving a faster temperature rise. Thus, a temperature difference should be apparent between the thin and the thick areas. Fig. 8b shows that some areas, such as the temple, the corner of the eyes and the mouth, and the forehead are thinner, whereas other areas such as the nose, the face, and the chin were thicker. Because the light source was not long enough to reach fully inside the artifact, the temperature of the crown area changed little.

The transmission step-heating thermography data, as illustrated in Fig. 8b, might also produce quantitative results of the wall thickness based on the aforementioned method. After fitting every data pixel with the theoretical Eq. (6), the thickness distribution over the entire imaged surface was obtained. Because the authors were not able to get an accurate diffusivity value of this old material, here the ordinary thermal diffusivity of the cast iron at 17.03 mm^2/s was applied [35]. Fig. 8c shows the calculated wall-thickness image of the Buddha head. There was a wide range of thickness variation for this Buddha head, from less than 2 mm at the corners of the eye and mouth, the temple, and forehead areas, to more than 25 mm at the nose area. Fig. 9 shows the experimental and fitting curves at three representative points from the

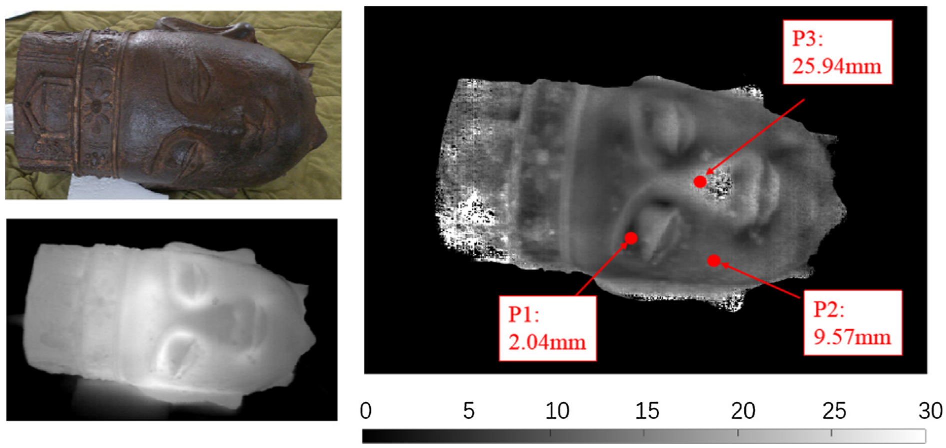

Fig. 8. (a) Photograph, (b) raw thermal image and (c) thickness image of the front view of the Buddha Head (thickness scale in mm).

corners of the eye (P1), face (P2) and nose (P3) area. For P1 which represents a thin area, the raw data fluctuated more than those at the other two points. This result can be attributed to two reasons. First, rust effects the diffusivity in a different way to the substrate material (i.e., cast iron). For thick areas, the thin surface layer of rust can be neglected but for thin areas it has a greater effect. Another reason for the fluctuation is lateral thermal diffusion. The temperature of thin areas is higher than that of surrounding thick areas; hence, as time passes the temperature difference rises and lateral diffusion becomes more pronounced. For this reason, the temperature at P1 was lower than expected at end of the test. The point P2 in Fig. 9 shows a perfect fitting state. However, the temperature rise at P3 was only 0.1 °C. This result indicates that the 6-s test duration was too short to resolve the thickness at the top of the nose area, which was even thicker than that at P3. This result is agreement with the estimate maximum thickness (3 cm) of the Buddha head.

Fig. 10 shows the experimental and analysis results for the two sides of the Buddha head. In general, these results are consistent with those in Fig. 8.

4. Conclusions

This study aimed to develop a method for evaluating the conditions of an ancient cast-iron Buddha head. The authors find that the transmission step-heating thermography is suitable for wall-thickness measurements. This work leads to the following conclusions:

The analytical results demonstrated the high accuracy of the step-heating thickness measurement method, with an error of less than 0.3%, for the thickness range from 5 to 50 mm. These results illustrate the capability of this method to analyze thick objects. Therefore, this method might complement traditional flash thickness measurement methods, which are more sensitive to thinner objects.

Experimental results for a 4-step-wedge SS304 sample were used to validate the application of the step-heating thickness measurement method. The measurement error decreased with thickness, from 5.6% for the thinnest step of 5 mm, to 1.4% for the second thinnest step at 11.4 mm, and finally to −0.1% for the thickest step at 24 mm. The error of the thin steps is mainly caused by the assumption of the temperature rise time of the halogen light and work is underway to address this. Nevertheless, this result illustrates that the method is effective for measuring thick objects.

The step-heating thermography method was successfully used to evaluate the condition of an ancient cast-iron Buddha head. The measurements provided detailed wall-thickness distributions over the entire casted head. These results will be valuable for researchers examining both cultural relic preservation and ancient iron casting processes.

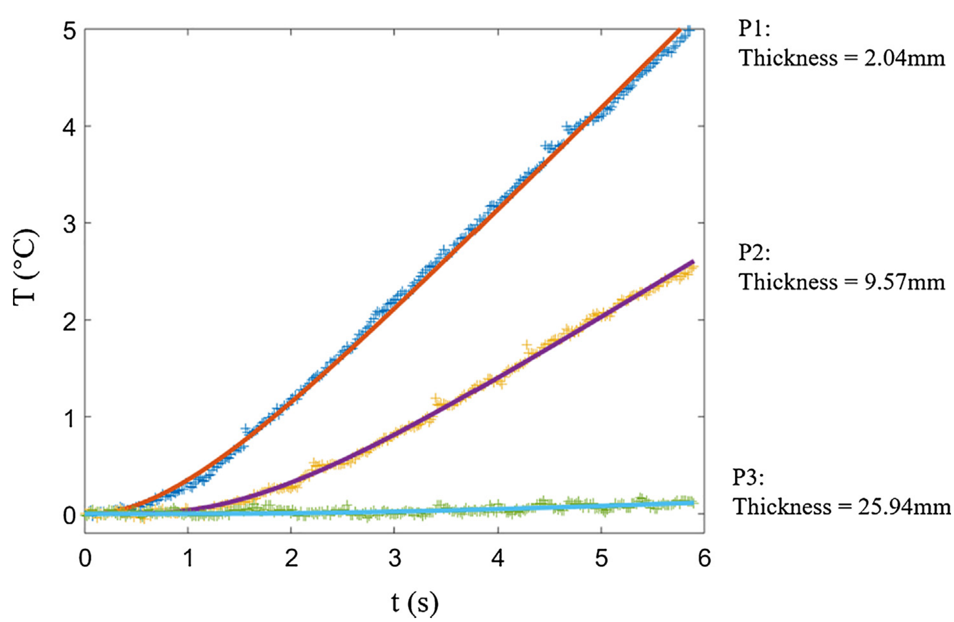

Fig. 9. Experimental and fitting curves at three representative surface points.

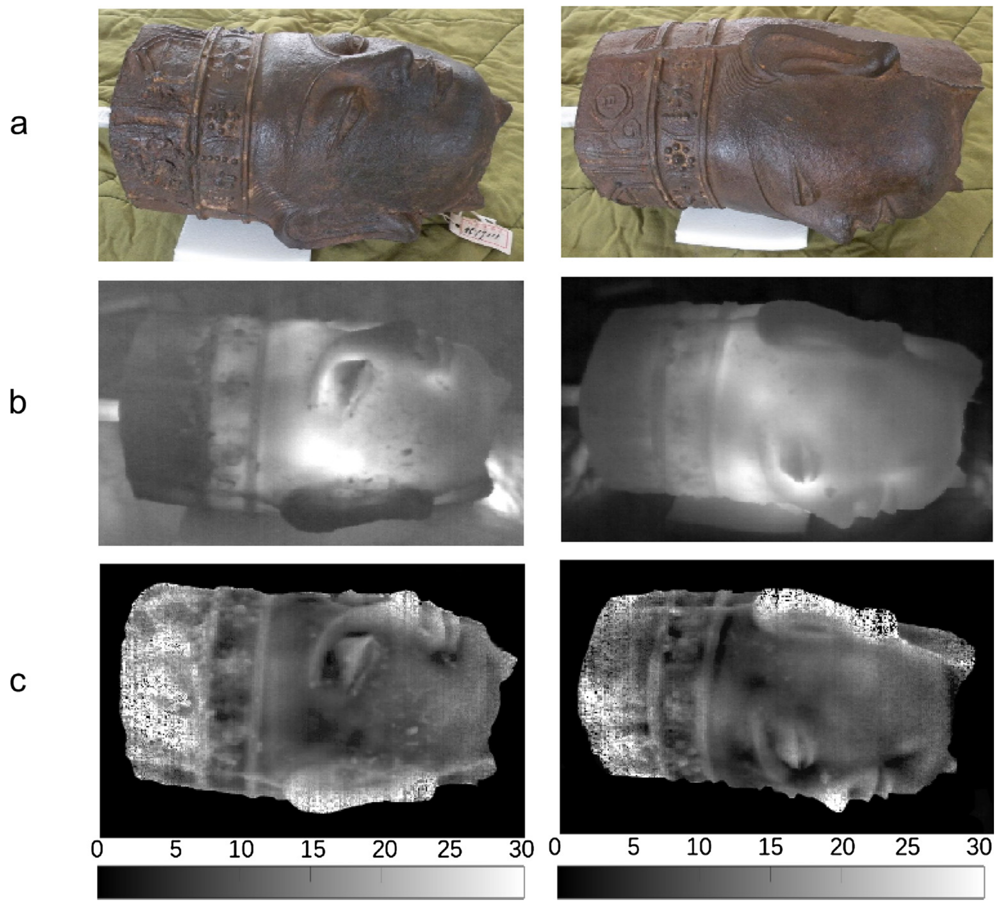

Fig. 10. (a) Photographs, (b) raw thermal images and (c) thickness images of the side views of the Buddha Head (thickness scale in mm).

Conflict of interest

The authors declared that there is no conflict of interest.

References

[1] M. Tortora, S. Sfarra, M. Chiarini, V. Daniele, G. Taglieri, G. Cerichelli, Non-destructive and micro-invasive testing techniques for characterizing materials, structures and restoration problems in mural paintings, Appl. Surf. Sci. 387 (2016) 971–985.
[2] C. Meola, R.D. Maio, N. Roberti, G.M. Carlomagno, Application of infrared thermography and geophysical methods for defect detection in architectural structures, Eng. Fail. Anal. 12 (2005) 875–892.
[3] C. Coupry, Application of Raman microspectrometry to arts objects, Analusis 28 (2000) 39–45.
[4] X. Maldague, Nondestructive Testing Handbook: Infrared and Thermal Testing, third ed., American Society for Nondestructive, 2001.
[5] A. Katunin, K. Dragan, M. Dziendzikowski, Damage identification in aircraft composite structures: a case using various non-destructive testing techniques, Compos. Struct. 127 (2015) 1–9.
[6] X. Li, J.G. Sun, N. Tao, L. Feng, J. Shen, Y. He, C. Zhang, An effective method to inspect adhesive quality of wind turbine blades using transmission thermography, J. Nondestructive Eval. 37 (2018) 19.
[7] T. Worzewski, R. Krankenhagen, M. Doroshtnasir, M. Röllig, C. Maierhofer, H. Steinfurth, Thermographic inspection of a wind turbine rotor blade segment utilizing natural conditions as excitation source, Part I: Solar excitation for detecting deep structures in GFRP, Infrared Phys. Technol. 76 (2016) 756–766.
[8] A. Kylili, P.A. Fokaides, P. Christou, S.A. Kalogirou, Infrared thermography (IRT) applications for building diagnostics: a review, Appl. Energ. 134 (2014) 531–549.
[9] F. Mercuri, U. Zammit, N. Orazi, S. Paoloni, M. Marinelli, F. Scudieri, Active infrared thermography applied to the investigation of art and historic artefacts, J. Therm. Anal. Calorim. 104 (2011) 475–485.
[10] E. Grinzato, P.G. Bison, S. Marinetti, Monitoring of ancient buildings by the thermal method, J. Cult. Herit. 3 (2002) 21–29.
[11] Lixin Wu, Shanjun Liu, Yuhua Wu, Infrared imaging detection of water permeation on field large-scale rock relics, IEEE Trans. Geosci. Remote Sens. 49 (2011) 581–590.
[12] Y.H. Jo, C.H. Lee, Quantitative modeling and mapping of blistering zone of the Magoksa Temple stone pagoda (13th century, Republic of Korea) by graduated heating thermography, Infrared Phys. Techn. 65 (2014) 43–50.
[13] J.L. Bodnar, J.C. Candore, J.L. Nicolas, G. Szatanik, V. Detalle, J.M. Vallet, Stimulated infrared thermography applied to help restoring mural paitings, NDT&E Int. 49 (2012) 40–46.
[14] S. Laureti, S. Sfarra, H. Malekmohammadi, P. Burrascano, D.A. Hutchins, L. Senni, G. Silipigni, X.P.V. Maldague, M. Ricci, The use of pulse-compression thermography for detecting defects in paintings, NDT&E Int. 98 (2018) 147–154.
[15] H. Zhang, S. Sfarra, K. Saluja, J. Peeters, J. Fleuret, Y. Duan, H. Fernandes, N. Avdelidis, C. Ibarra-Castanedo, X. Maldague, Non-destructive investigation of paintings on canvas by continuous wave terahertz imaging and flash thermography, J. Nondestructive Eval. 36 (2017) 34.
[16] Hai Zhang, Stefano Sfarra, Ahmad Osman, Clemente Ibarra-Castanedo, Panagiotis Theodorakeas, Nicolas P. Avdelidis, Maria Koui, Domenica Paoletti, Xavier P. V. Maldague, Nondestructive Investigation of Paintings on Canvas by Infrared Thermography, Air-Coupled Ultrasound, and X-Ray Radiography, in: 10th International Symposium on the Conservation of Monuments in the Mediterranean Basin (MONUBASIN), 20–22 of September 2017, Athens, Greece.
[17] P. Tavakolian, S. Sfarra, G. Gargiulo, K. Sivagurunathan, A. Mandelis, Photothermal coherence tomography for 3-D visualization and structural non-destructive imaging of a wood inlay, Infrared Phys. Techn. 91 (2018) 206–213.
[18] N. Orazi, S. Paoloni, U. Zammit, C. Cicero, M. Ferretti, G. Caruso, O. Colacicchi Alessandri, R. Paris, F. Mercuri, Thermographic investigation of bronze artefacts: characterization of structure elements and casting faults in masterpieces of the Bronze Statuary of Rome, Int. J. Thermophys. 39 (2018) 141.
[19] F. Mercuri, G. Caruso, N. Orazi, U. Zammit, C. Cicero, O. Colacicchi Alessandri, M. Ferretti, S. Paoloni, Interface thermal conductance characterization by infrared thermography: a tool for the study of insertions in bronze ancient Statuary, Infrared Phys. Techn. 90 (2018) 31–39.
[20] D. Ambrosini, A. Paoletti, D. Paoletti, S. Sfarra, Ndt methods in artwork corrosion monitoring, Proc. of SPIE 6618 (2007) 661817.
[21] Y. Song, X. Han, Effect of driving frequency on non-linear coupling between ultrasound transducer and target under inspection in Sonic Infrared Imaging, Infrared Phys. Technol. 66 (2014) 43–48.
[22] K. Chatterjee, S. Tuli, S.G. Pickering, D.P. Almond, A comparison of the pulsed, lock-in and frequency modulated thermography nondestructive evaluation techniques, NDT&E Int. 44 (2011) 655–667.
[23] X. Xiao, B. Gao, Woo W. Lok, G. Tian, T. Xiao, Spatial-time-state fusion algorithm for defect detection through Eddy current pulsed thermography, Infrared Phys. Technol. 90 (2018) 133–145.

[24] H.D. Benitez, C. Ibarra-Castanedo, A. Bendada, X. Maldague, H. Loaiza, E. Caicedo, Definition of a new thermal contrast and pulse correction for defect quantification in pulsed thermography, Infrared Phys. Technol. 51 (2008) 160–167.
[25] Z. Zeng, J. Zhou, N. Tao, L. Feng, C. Zhang, Absolute peak slope time based thickness measurement using pulsed thermography, Infrared Phys. Technol. 55 (2012) 200–204.
[26] W.J. Parker, R.J. Jenkins, C.P. Butler, G.L. Abbott, Flash method of determining thermal diffusivity, heat capacity, and thermal conductivity, J. Appl. Phys. 32 (1961) 1679–1684.
[27] D.L. Balageas, Thickness or diffusivity measurements from front-face flash experiments using the TSR (thermographic signal reconstruction) approach, in: Proc. QIRT 2010 Conference, Quebec City, Quebec, Canada, 2010.
[28] ASTM Standard E2582-07, Standard Practice for Infrared Flash Themography of Composite Panels and Repair Patches Used in Aerospace Applications, ASTM International, West Conshohocken, 2007.
[29] J. Hua, Ancient Chinese metal technology, Elephant press, Zhengzhou, 1999 (in Chinese).
[30] C. Wang, The Ancient Aiant Iron Buddhist Sculpture, Res. Stud. Foundry Equip. 4 (2006) 40–45 (in Chinese).
[31] H.S. Carslaw, J.C. Jaeger, 1959 Conduction of Heat in Solids, second ed., Oxford University Press, 1959, p. 112.
[32] X. Li, N. Tao, J.G. Sun, C. Zhang, Y. Zhao, Thickness measurement by two-sided step-heating thermal imaging, Rev. Sci. Instrum. 89 (2018) 014902.
[33] X. Li, J.G. Sun, N. Tao, Z. Zeng, Y. Zhao, J. Shen, C. Zhang, Application of nonlinear data fitting method to thermal diffusivity of carbon-carbon composite measured by transmission pulsed thermography, Acta Phys. Sin. 66 (18) (2017) 188702 (in Chinese).
[34] X. Song, J. An, Xinbian Zhongwai Jinshu Cailiao Shouce, Chemical Industry Press, Beijing, 2008 (in Chinese).
[35] C.P. Kothandaraman, S. Subramanyan, Heat and Mass Transfer Data Book, New Academic Science, London, 2013 contd. 6.
[36] N. Shi, X. Wang, C. Zhang, The application of infrared thermal wave imaging in conservation, J. National Museum China 166 (2017) 149–157 (in Chinese).
[37] Maria C. Di Tuccio, Nicola Ludwig, Marco Gargano, Adriana Bernardi, Thermographic inspection of cracks in the mixed materials statue: Ratto delle Sabine, Heritage, Science 3 (2015) 10.